A Bidirectional Wireless Power Transfer System for Roadway Powered Electric Vehicles

Johannes A. Russer[1], Marco Dionigi[2], Mauro Mongiardo[2], and Peter Russer[1]

***Abstract*—A wireless power transfer system for roadway powered electric vehicles (EVs) is presented. The system concept is using inductive coupling of primary coils arranged in a linear array in the roadway to secondary coils in each EV. The system is geared to minimize loss of the stored energy in the primary coils and compensation capacitors by passing the energy on to the subsequent coil and capacitor of the linear array. The inductive power transfer (IPT) system is operated as a switched resonant inverter controlled by the primary and secondary coil currents. By this way power transfer in both directions can be accomplished. We describe an extension of the moving field inductive power transfer (MFIPT) system by introducing a synchronous switched DC-DC converter. A rectangular AC power supply voltage is provided by a switched inverter from the underroad DC power supply. An automatic switching adapts to load changes and switches in optimum phase. Also the analysis of a basic IPT cell is discussed and efficiency considerations are given.**

***Index Terms*—wireless power transfer, inductive power transfer, efficiency, electric vehicles, switched DC-DC converter.**

I. Introduction

Since a few years electric powered vehicles are available on the market, developed with the goal to supersede cars with combustion engines. If powered by electrical energy from renewable sources, EVs may be a solution to the problems which we are facing due to limited resources of fossil fuel and environmental concerns. At the present time, most EVs are battery powered and the cars suffer from short cruising range, long charging times or the need to exchange the depleted battery for a charged one, high cost and the heavy weight of the battery. Wireless inductive power transfer offers an interesting option for powering EVs. Inductive power transfer (IPT) systems have already been suggested for contact-less battery charging of cars, usually as stationary systems for parked cars, e.g. in [1]–[3]. These works give an account of the problem of compensation of the stray inductances of a loosely coupled IPT system. In [4], [5], design methodologies for loosely coupled IPT systems are discussed.

High efficiency can be achieved in power transfer under loose coupling conditions by an appropriate tuning of the resonant circuits. The capacitive compensation of the leakage inductance yields a high quality factor and considerable energy storage in the resonant circuits formed by the coils and the compensation capacitors.

Roadway powering, as proposed in [6]–[9], may overcome aforementioned problems of limited cruising range, long battery charging times, high cost and heavy weight of batteries.

[1]Institute for Nanoelectronics, Technische Universität München, Arcisstrasse 21, 80333 Munich, Germany, e-mail: jrusser@tum.de, russer@tum.de
[2]Università di Perugia, Dipartimento di Ingegneria, Via G. Duranti, 93, 06125 Perugia, Italy, e-mail: mongiardo@diei.unipg.it, dionigi@diei.unipg.it

In 1978, Bolgar et al. already have suggested inductive roadway powering of electric vehicles using a power-coupling arrangement which is essentially a wide-airgap transformer [6], [7]. The power source is a sequence of coils consisting of laminated transformer iron surrounded with suitable windings. The pickup mounted in the electric vehicle is of similar construction as the source.

Using directly resonant magnetic Wireless Power Transfer (WPT) significantly extends the range of applicability of IPT [10]–[13]. We already have described in [14] a moving field inductive power transfer (MFIPT) system based on stationary primary coils linearly arranged along one or several tracks on a roadway and a secondary coil in every vehicle moving along the track. Fig. 1 shows the schematic of the MFIPT system. The vehicle is equipped with a secondary coil mounted at the bottom of the car chassis. The primary coils are installed below the road surface.

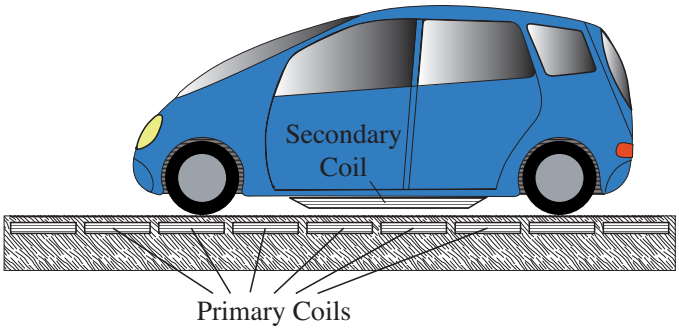

Fig. 1: Schematic of the MFIPT system

Fig. 2 shows the schematic arrangement of the primary coils forming the sources and secondary coil forming the pickup. The cross-section of sources and pickup follows the design of Bolgar et al [6], [7]. The secondary coil has a length extension $l_2 > 2l_1 + a$ where l_1 is the lengths of the primary coils and

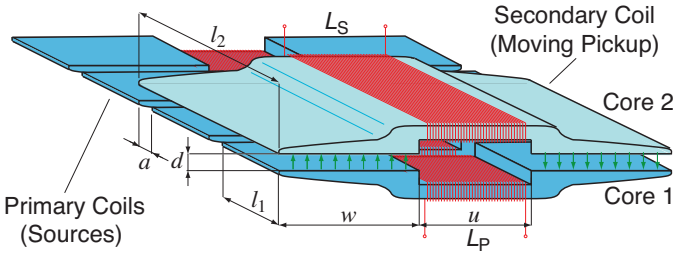

Fig. 2: Sources and pickup

a is the spacing between the primary coils. So at any time the secondary coil covers at least one primary coil. Cores 1 and 2 of the coils 1 and 2 form together the core of a transformer with wide air gaps. A large width w is chosen in order to achieve a low magnetic reluctance of the magnetic circuit formed by the two cores 1 and 2 and the two air gaps. For sufficiently large air gap width and sufficiently high permeability of the cores the magnetic reluctance depends only on the gap width d and the cross sectional area $l_1 w$. The magnetic flux Φ in the transformer is given by

$$\Phi = \frac{\mu_0 l_1 w}{d}(n_1 i_1 + n_2 i_2)\,, \tag{1}$$

where i_1 and i_2 are the primary and secondary loop currents and n_1 and n_2 are the primary and secondary numbers of windings. Under neglection of the stray inductances, the primary and secondary coil voltages v_1 and v_2 are given by

$$v_1 = n_1 \frac{d\Phi}{dt}\,, \quad v_2 = n_2 \frac{d\Phi}{dt}\,. \tag{2}$$

So far we have neglected the stray inductance of the transformer.

At any time for every moving EV only one primary coil is active. The primary coil is fully covered by the secondary coil and excites an alternating magnetic field which induces voltage in the secondary coil. For a short time interval the secondary coil of the moving car covers two primary coils. Within this time interval the activation is passed over to the next primary coil unit in such a way that the energies stored in the primary coil and its compensation capacitor are transferred to the subsequent coil and the respective compensation capacitor. This transfer is performed in a short time and without energy loss.

In [15] we have described a MFIPT with a synchronous switched switched resonant inverter, where the rectangular AC power supply voltage is tapped from the under-road DC power supply via a switched inverter [16]–[20]. The inverter is switched synchronously with the primary coil current. The advantage of this solution is that the switched oscillator automatically is adapting to load changes and switches in optimum phase.

In [21] we presented a further extension of the MFIPT system by introducing a switched inverter also in the secondary circuit. By this way power transfer in both directions can be accomplished. Under forward operation, when the DC line is delivering power to the electric vehicle the switched inverter in the secondary circuit is operated as a synchronously switched rectifier.

II. Operation of the MFIPT System

Fig. 3 shows the schematic of the MFIPT system. The MFIPT system exhibits the stationary primary loops $L_{P1}, L_{P2}, L_{P3}, L_{P4}, \ldots$ and the moving secondary loop L_S. $C_{P1}, C_{P2}, C_{P3}, C_{P4}, C_{P5}, \ldots$ are compensation capacitors for compensation of the stray inductance of the primary loops, and C_S the compensation capacitor for the compensation of the secondary loop. The switches S_{Li} and S_{Ri}, respectively, with $i = 1, 2, 3, \ldots$ connect the primary loops L_{Pi} either with the compensation capacitors C_{Pi} or with C_{Pi+1}. The MFIPT system is DC-powered by the two power lines at potentials $+V_0$ and $-V_0$, respectively. The pump switches S_{Pi} can be toggled with a frequency $f_T = 1/T$ between $+V_0$ and $-V_0$ and apply a rectangular voltage pulse, shown in Fig. 4, to the primary loop S_{Li}. For the non-activated primary loops the respective switches S_{Li} are remaining in a rest position.

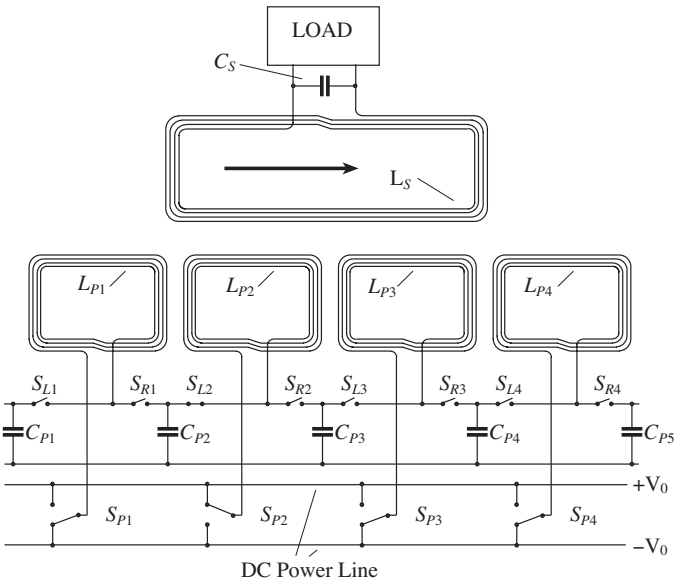

Fig. 3: Schematic of the MFIPT system

At any instant, only one single primary coil is active per EV. Its alternating magnetic field induces a voltage in the secondary coil. The primary coil is active while there is a full overlap with the secondary coil located in the EV. At the instant when the secondary coil of the EV has overlap with two primary coils in the roadway, the activation is handed over to the subsequent primary coil. This is done such that energies stored in the primary coil and its compensation capacitor are transferred to the next primary coil and its compensation capacitor. No energy is lost when it is transferred from one primary coil to the subsequent primary coil.

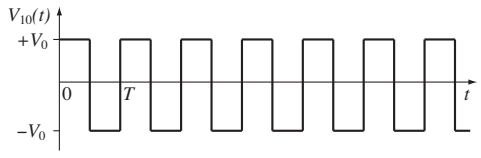

Fig. 4: Pump pulse wavefom

To explain the operation of the MFIPT system we start with an initial state of the system where only the primary coil L_{P2} is activated. The primary coil L_{P2} is connected via the closed switch S_{L2} with the compensation capacitor C_{P2}, so that L_{P2} and C_{P2} are forming a series resonant circuit. This series resonant circuit is AC powered via the rectangular voltage pulse train generated by the pump switch S_{P2}. The described circuit forms an IPT basic cell as depicted in Figs. 9 and 11. The dynamics of the basic cell will be investigated in Section VI. Arrangements similar to this basic cells already

have been discussed in literature for stationary IPT systems with a single localized primary cell [3], [22]–[24].

In the state depicted in Fig. 3 the secondary coil already covers not only the primary coil L_{P2} but also the subsequent primary coil L_{P3}. Therefore L_{P3} can now be activated and L_{P2} can be turned off. To accomplish this change, the capacitor C_{P2} will be replaced by the capacitor C_{P3} in the primary resonant circuit $L_{P2}C_{P2}$ in a first step. This is done at the moment when all energy of the resonant circuit is stored in L_{P2}, i.e. when the magnitude of the current through L_{P2} assumes a maximum value and the voltage across C_{P2} is zero. At this moment the switch S_{R2} will be closed and immediately after this the switch S_{L2} will be opened such that the current through L_{P2} is not interrupted. The resonant circuit $L_{P2}C_{P2}$ now is replaced by the resonant circuit $L_{P2}C_{P3}$ and in the following the energy is converted between magnetic energy stored in L_{P2} and electric energy stored in C_{P3}.

In a subsequent step, the loop L_{P2} is replaced by the loop L_{P3}. This is done at the moment when all energy of the resonant circuit $L_{P2}C_{P3}$ is stored in the capacitor C_{P3}. In this moment the magnitude of the voltage across C_{P3} exhibits a maximum value and the current through L_{P2} is zero. So, at this moment the switch S_{R2} will be opened and the switch S_{L3} will be closed. At this time also the pump switch S_{P2} goes into its rest position and the pump switch S_{P3} now will be activated and toggled with the frequency f_T.

The two-step procedure described above moves the energy to the subsequent IPT cell irrespective of the long transient times of the IPT cells due to the quality factors of the resonant circuits. In the next section we analyze the basic cell of the inductive power transfer (IPT) system. For this analysis we only consider a single primary loop. The analysis, however is representative for the operation of the whole MFIPT system, since the replacement of the capacitors by the subsequent ones in their zero voltage state and the replacement of the primary loops by the subsequent ones in their zero current state does not influence the dynamics. We only have to replace the voltages and currents, respectively, by the voltages and currents of the subsequent elements.

III. Analysis of the IPT Basic Cell

The analysis of a basic IPT cell, as presented in this section, allows in a straightforward manner for the description of the whole MFIPT system. Since dynamics are not influenced when we substitue one of the capacitors by the subsequent ones while in their zero voltage state and, accordingly, when we replace one of the primary loops by the subsequent one in their zero current state, we only have to replace the voltages and currents, respectively, by the voltages and currents of the element of the subsequent cell. The circuit schematic of the basic IPT cell is given in Fig. 5.

A description for the voltages and currents is given in the Laplace domain by

$$V_{10} = \left(sL_P + \frac{1}{sC_P} + R_P\right) I_1 + sMI_2\,, \tag{3a}$$

$$0 = sMI_1 + \left(sL_S + \frac{1}{sC_S} + R_S + R_L\right) I_2\,, \tag{3b}$$

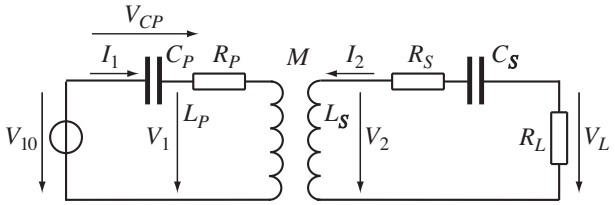

Fig. 5: The harmonically driven IPT basic cell

where s is the complex frequency, L_P, L_S, and M are the inductances and R_P and R_S are the series loss resistors of the primary and secondary coils and their mutual inductance, respectively, C_P and C_S are the capacitances of the primary and secondary compensation capacitors, and G is the load conductance. Zero voltages and currents are assumed for the inital state. $V_{10}(s)$ is the driving voltage. We assume that primary and secondary resonant circuits are tuned to the same angular resonant frequency

$$\omega_r = \frac{1}{\sqrt{L_P C_P}} = \frac{1}{\sqrt{L_S C_S}} \tag{4}$$

and we introduce the coupling factor

$$k = \frac{M}{\sqrt{L_P L_S}}\,, \tag{5}$$

the damping coefficients

$$\alpha_P = \frac{R_P}{L_P}\,,\ \alpha_S = \frac{R_S + R_L}{L_S}\,,\ \alpha_L = \frac{R_L}{L_S}\,, \tag{6}$$

and the turns ratio

$$n = \sqrt{\frac{L_S}{L_P}}\,. \tag{7}$$

From (3a) and (3b), we obtain

$$\frac{1}{\sqrt{L_S L_P}} V_{10} = \frac{1}{n}\left(s + \frac{\omega_r^2}{s} + \alpha_P\right) I_1 + skI_2\,, \tag{8a}$$

$$0 = skI_1 + n\left(s + \frac{\omega_r^2}{s} + \alpha_S\right) I_2\,. \tag{8b}$$

The current $I_1(s)$ through the primary loop is

$$I_1(s) = \frac{s + \frac{\omega_r^2}{s} + \alpha_S}{\left[\left(s + \frac{\omega_r^2}{s} + \alpha_P\right)\left(s + \frac{\omega_r^2}{s} + \alpha_S\right) - s^2k^2\right] L_P} V_{10}(s). \tag{9}$$

The voltage $V_{CP}(s)$ across the primary compensation capacitor C_P is

$$V_{CP}(s) = \frac{\omega_r^2\left(s + \frac{\omega_r^2}{s} + \alpha_S\right)}{s\left[\left(s + \frac{\omega_r^2}{s} + \alpha_P\right)\left(s + \frac{\omega_r^2}{s} + \alpha_S\right) - s^2k^2\right]} V_{10}(s)\,. \tag{10}$$

The current $-I_2(s)$ flowing from the secondary loop is

$$I_2(s) = \frac{-snk}{\left[\left(s + \frac{\omega_r^2}{s} + \alpha_P\right)\left(s + \frac{\omega_r^2}{s} + \alpha_S\right) - s^2k^2\right] L_S} V_{10}(s). \tag{11}$$

The voltage $V_L(s)$ provided across the load R_L is given by

$$V_L(s) = \frac{s\,\alpha_L n k}{\left(s+\frac{\omega_r^2}{s}+\alpha_P\right)\left(s+\frac{\omega_r^2}{s}+\alpha_S\right)-s^2k^2} V_{10}(s)\,. \tag{12}$$

IV. Efficiency Considerations

For an inductive power transfer system the efficiency η, defined as the ratio of the power P_L delivered to the load to the power P_{in} flowing from the source into the wireless power transfer two-port has to be optimized:

$$\eta = \frac{P_L}{P_{in}} \tag{13}$$

We keep in mind that for a high power transmission system the source impedance should be small in comparison with the input impedance of the primary loop circuit. Otherwise the load would reduce the source voltage and moreover would give rise to power loss in the source. Complex conjugate power matching is not an issue for power transmission systems.

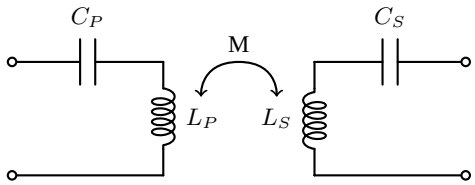

Fig. 6: Coupled inductances and resonant capacitances equivalent network

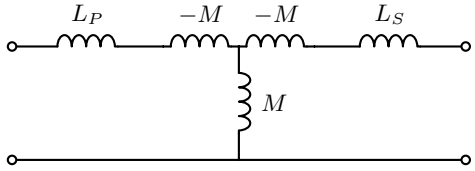

Fig. 7: Coupled inductances equivalent network: Tee representation. The central part, with the series inductors $-M$ and the parallel inductor M, realizes an immittance inverter

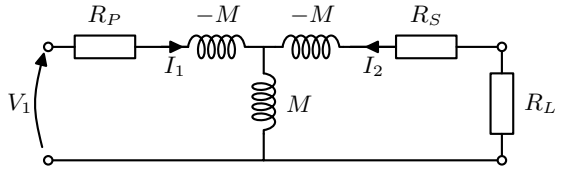

Fig. 8: Network used for computing the efficiency of coupled inductances. The inductances have been removed (absorbed into the matching network) and R_g, R_L are source and load impedances

The power transfer two-port consists of primary and secondary coils with primary and secondary inductances L_P and L_S, respectively, and the mutual inductance M. The series resistances are R_P and R_S, respectively. Assuming that primary and secondary inductances are compensated by capacitors C_P and C_S, respectively, the coupling two-port is an immittance inverter with additional series resistances at both ports. We assume that primary and secondary circuit satisfy the resonance condition (4).

At the resonant frequency ω_r the coupling-twoport is described by the admittance matrix

$$\boldsymbol{Z}_c = \begin{bmatrix} R_P & \jmath\omega_r M \\ \jmath\omega_r M & R_S \end{bmatrix}. \tag{14}$$

We obtain

$$V_1 = R_P I_1 + \jmath\omega_r M I_2\,, \tag{15a}$$

$$0 = \jmath\omega_r M I_1 + (R_S + R_L) I_2\,. \tag{15b}$$

This yields

$$I_1 = \frac{R_S + R_L}{R_P(R_S+R_L)+\omega_r^2 M^2} V_1\,, \tag{16}$$

$$I_2 = \frac{-\jmath\omega_r M}{R_P(R_S+R_L)+\omega_r^2 M^2} V_1\,. \tag{17}$$

The active power P_{in} flowing into the primary coil is given by

$$P_{in} = \frac{1}{2}\Re\{V_1 I_1^*\} = \frac{R_S+R_L}{R_P(R_S+R_L)+\omega_r^2M^2}|V_1|^2\,. \tag{18}$$

The active power P_L flowing into the load resistance R_L is given by

$$P_L = \frac{1}{2}R_L|I_2|^2 = \left[\frac{\omega_r M}{R_P(R_S+R_L)+\omega_r^2M^2}\right]^2 R_L|V_1|^2\,. \tag{19}$$

Inserting (18) and (19) into (13) yields

$$\eta = \frac{\omega_r^2 M^2 R_L}{R_P R_S^2}\,\frac{1}{\left(1+\frac{R_L}{R_S}\right)\left[\left(1+\frac{R_L}{R_S}\right)+\frac{\omega_r^2M^2R_L}{R_PR_S}\right]}\,. \tag{20}$$

The efficiency would go to $\eta \to 1$ for $|M| \to \infty$, however, this also would yield a quality factor going to infinity. Therefore high efficiency would yield narrow bandwidth and high sensitivity with respect to parameter variations.

With the the quality factors Q_i given by

$$Q_i = \frac{\omega_r L_i}{R_i} \text{ for } i = P, S\ , \tag{21}$$

and the coupling coefficient k defined in (5) we introduce the normalized parameters

$$\chi = \frac{\omega_r^2 M^2}{R_P R_S} = k^2 Q_P Q_S\,, \tag{22a}$$

$$x = \frac{R_L}{R_S}\,, \tag{22b}$$

and write equation (20) in the normalized form

$$\eta = \frac{x}{1+x}\,\frac{\chi}{1+x+\chi}\,. \tag{23}$$

We would like to find out for what value of the variable x the efficiency is maximized. To this end we consider (23) and we take its derivative with respect to x. The positive solution is

$$x = \sqrt{\chi+1}\,, \tag{24}$$

which, once back substituted into (23), provides the following expression for the maximum efficiency η_{max}

$$\eta = \frac{\chi}{\left(\sqrt{\chi+1}+1\right)^2}\,. \tag{25}$$

This equation defines the termination impedance R_{Lmax} for maximum efficiency as

$$R_{Lmax} = R_S\sqrt{k^2 Q_P Q_S + 1}\,. \tag{26}$$

It is also noted that the termination impedance for maximum efficiency R_{Lmax} determines the input impedance R_{in}. By straightforward substitutions we obtain:

$$R_{in} = R_P\sqrt{\chi + 1}\,. \tag{27}$$

In other words, the lossy coupled inductors network has as reference impedance at port 1, $R_{01} = R_{in}$ and as reference impedance at port 2 $R_{02} = R_{Lmax}$.

V. The Unidirectional Switched Power Inverter

Switched inverter circuits based on a load-adaptive modulated phase already have been described in literature [16]–[19]. Fig. 9 shows the basic cell of a switched inverter IPT system. The sinusoidal waveform generator in Fig. 5 has been replaced by the toggled switch S_P. Compared to a sinusoidal AC power source, the switched inverter has the advantage of a high conversion efficiency. Furthermore, the inverter can be switched synchronously with the primary coil current, so that the frequency of the switched oscillator automatically adapts to the resonant frequency changes of the IPT system due to load changes and switches in optimum phase. Switching between

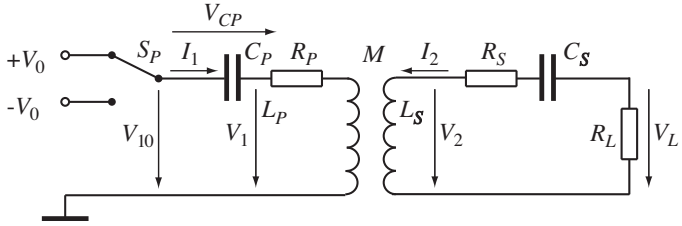

Fig. 9: The switched inverter IPT basic cell

$+V_0$ and $-V_0$, a pulsed waveform with a time dependence as depicted in Fig. 4 is generated.

For the representation of the pulsed waveform with a frequency $f_T = 1/T$ in the Laplace domain we find [25, p. 246]

$$V_{10}(s) = \frac{1 - \mathrm{e}^{-sT/2}}{s\left(1 + \mathrm{e}^{-sT/2}\right)}\,. \tag{28}$$

Fig. 10 shows the transient time dependence of the load voltage $v_L(t)$.

For the analytic treatment of the switched inverter IPT system in the Laplace domain we also refer to [14] where the case of a parallel resonant circuit incorporating the secondary loop was treated. In our further considerations, however, we will treat the switched inverter problem in time domain using a state equation approach.

VI. The Bidirectional Switched Power Inverter

Fig. 11 shows the basic cell of the IPT system. The IPT basic cell consists of a full-bridge switched inverter and a resonant transformer. Bidirectional switched inverter circuits allow to enforce power transfer in both directions. In the bidirectional

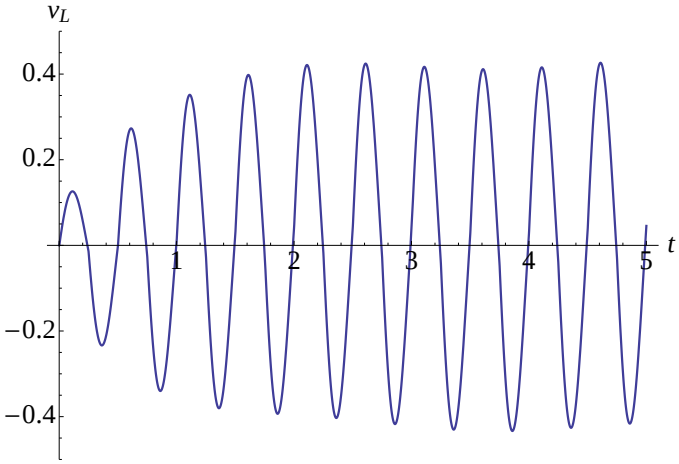

Fig. 10: Voltage $v_L(t)$ across the load

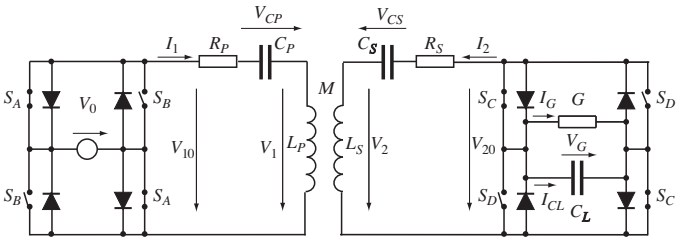

Fig. 11: The bidirectional inverter basic cell

switched inverter circuit the rectifier on the secondary side is replaced by controlled switches [26]–[28].

The full-bridge switched inverters on the primary and secondary sides consist of the four switches S_A, S_B on the primary side and the four switches S_C, S_D on the secondary side. It is operated such that either the switches S_A are closed and the switches S_B are open or vice versa. The switched inverter is controlled by the primary loop current $i_1(t)$. The MFIPT system is DC-powered by the two power conductors with the potential difference V_0.

The action of the switches is described by

$$v_{10}(t) = \zeta V_0 \operatorname{sign} i_1(t)\,, \tag{29a}$$

$$v_{20}(t) = -\zeta v_G(t) \operatorname{sign} i_2(t)\,, \tag{29b}$$

$$i_{CL}(t) = -G v_G(t) - \zeta i_2(t) \operatorname{sign} i_2(t)\,, \tag{29c}$$

where the sign function exhibits the values ± 1 depending on whether the sign of the argument is positive or negative. The primary inverter switches S_A and S_B and the secondary inverter switches S_C and S_D are controlled by the primary loop current I_1 and the secondary loop current I_2, respectively. We use small letters to denote time dependent variables such as $i(t)$, and capital letters for variables in the Laplace domain. The control parameter $\zeta = \pm 1$ has to be set to $+1$ when the power flow shall be directed from the DC supply line on the primary side to the electric vehicle on the secondary side. Setting $\zeta = -1$ enforces the power flow direction from the secondary side to the primary side. Changing the phase of the switched inverters by $180°$ reverses the power flow direction and the EV battery/capacitor is transferring power back to the primary DC feed line. This is an interesting option when

breaking the EV and no further battery charging is required.

Naturally, when the coils are coupled, the operating frequency changes. In order to cope with this behavior we have the following possibilities:

1) to use a source which adaptively move in frequency (the Royer oscillator is a good candidate and has been investigated in [29]);
2) to employ a control system that sets the oscillating frequency to the new appropriate value;
3) to introduce appropriate matching networks that, by selecting proper element values, keep the resonant frequency fixed.

The last approach has the advantage that, if we have a system using a resonant switched inverter, we can keep the resonant inverter switching frequency fixed while we can adjust the resonant frequency in order to maximize power exchange.

As the state variables of the circuit we choose the inductor currents $i_1(t)$ and $i_2(t)$ and the capacitor voltages $v_{CP}(t)$ and $v_2(t)$. For these variables we obtain the state equations

$$\frac{dv_{CP}}{dt} = \frac{1}{C_P} i_1 \,, \tag{30a}$$

$$\frac{dv_{CS}}{dt} = \frac{1}{C_S} i_2 \,, \tag{30b}$$

$$\frac{dv_G}{dt} = \frac{1}{C_L} i_{CL} \,, \tag{30c}$$

$$\frac{di_1}{dt} = \frac{v_{10} - R_P i_1 - v_{CP}}{(1-k^2)L_P} - \frac{k(v_{20} - v_{CS})}{(1-k^2)nL_P} \,, \tag{30d}$$

$$\frac{di_2}{dt} = -\frac{k(v_{10} - v_{CP})}{(1-k^2)nL_P} + \frac{v_{20} - R_S i_2 - v_{CS}}{(1-k^2)n^2 L_P} \,. \tag{30e}$$

We assume primary and secondary resonant circuits to be tuned to the same angular resonant frequency, given by (4).

We introduce the damping factor

$$\beta \equiv 1/Q = \frac{G}{\omega_r C_L} \,, \tag{31a}$$

the normalized load capacitor

$$\gamma = \frac{C_L}{C_P} \,, \tag{31b}$$

and the normalized time

$$\tau = \omega_r t \,. \tag{31c}$$

The coupling factor k and the turns ratio n are given in (5) and (7).

We use the normalized variables $x_1 \ldots x_5$ given by

$$\begin{aligned} x_1 &= -\frac{v_{CP}}{V_0} \,,\; x_2 = \frac{v_{CS}}{V_0} \,, \\ x_3 &= \frac{\omega_r L_P i_1}{V_0} \,,\; x_4 = \frac{\omega_r L_P i_2}{V_0} \,, \\ x_5 &= \frac{v_G}{V_0} = \frac{i_G}{GV_0} \,, \end{aligned} \tag{32a}$$

the normalized resistors $r_1 = R_P/\omega_r L_P$, $r_2 = R_S/\omega_r L_P$, and obtain the normalized state equations

$$\frac{d\boldsymbol{x}}{d\tau} = \boldsymbol{A}\boldsymbol{x} + \xi \operatorname{sign} x_3 \boldsymbol{B} + \xi \operatorname{sign} x_4 \boldsymbol{C}\boldsymbol{x} \tag{33}$$

with

$$\boldsymbol{A} = \begin{bmatrix} 0 & 0 & -1 & 0 & 0 \\ 0 & 0 & 0 & -n^2 & 0 \\ \frac{1}{(1-k^2)} & \frac{-k}{(1-k^2)n} & \frac{-r_1}{(1-k^2)} & 0 & 0 \\ \frac{-k}{(1-k^2)n} & \frac{1}{(1-k^2)n^2} & 0 & \frac{-r_2}{(1-k^2)n^2} & 0 \\ 0 & 0 & 0 & 0 & -\beta \end{bmatrix} ,$$

$$\boldsymbol{B} = \begin{bmatrix} 0 \\ 0 \\ \frac{1}{(1-k^2)} \\ \frac{-k}{(1-k^2)n} \\ 0 \end{bmatrix} , \tag{34}$$

$$\boldsymbol{C} = \begin{bmatrix} 0 & 0 & 0 & 0 & 0 \\ 0 & 0 & 0 & 0 & 0 \\ 0 & 0 & 0 & 0 & \frac{k}{(1-k^2)n} \\ 0 & 0 & 0 & 0 & \frac{-1}{(1-k^2)n^2} \\ 0 & 0 & 0 & \gamma^{-1} & 0 \end{bmatrix} .$$

We consider as an example example of the transient and steady state behavior of the MFIPT system for the parameters $k = 0.7$, $\beta = 10^{-3}$, $\gamma = 100$, $r_1 = r_2 = 0.1$. For forward power transfer we set $\zeta = 1$. Fig. 12 shows the transients of the normalized primary and secondary compensation capacitor voltages $x_1(\tau)$ and $x_2(\tau)$, the normalized primary and secondary loop currents $x_3(\tau)$ and $x_4(\tau)$, and the load voltage $x_5(\tau)$. At the onset of the oscillations the primary and secondary switches controlled by the primary and secondary currents are nearly in phase.

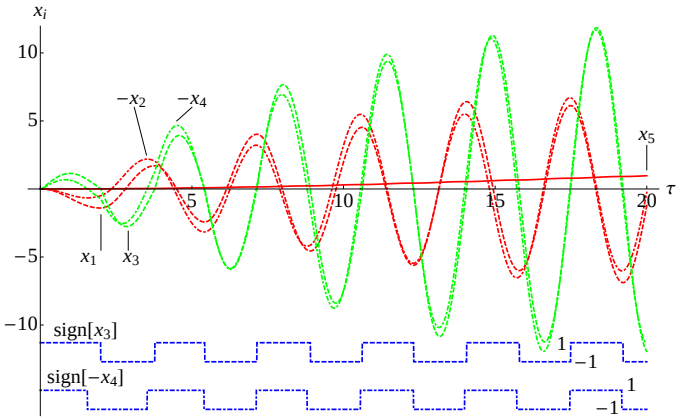

Fig. 12: Transients of the normalized voltages and currents $x_1(\tau)$, $x_2(\tau)$, $x_3(\tau)$, $x_4(\tau)$ and $x_5(\tau)$

Fig. 12 shows the system approaching the steady state. There is a considerable phase delay between the primary and secondary switches, limiting the power flow.

VII. The Power Transfer to the Electrical Vehicle

As an example let us consider the case of two coils, that may be suitable for EV applications, with diameter 1500 mm and height of 50 mm composed of 6 wire turns; such coils present an inductance of 110 μH. The coupling coefficient k changes with their distance; for a center distance (in mm) of

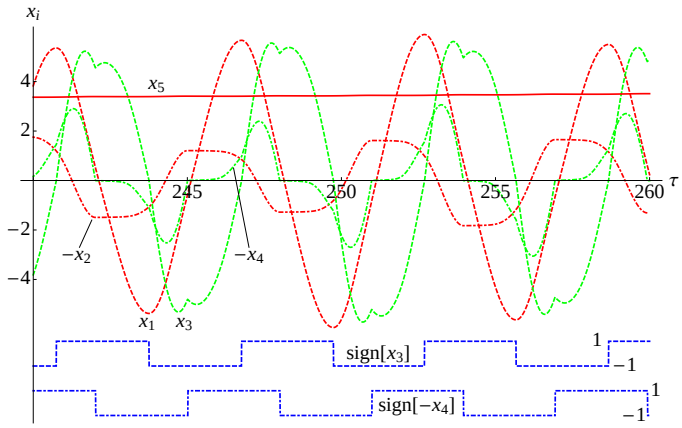

Fig. 13: Approaching the steady state of the normalized voltages and currents $x_1(\tau)$, $x_2(\tau)$, $x_3(\tau)$, $x_4(\tau)$ and $x_5(\tau)$

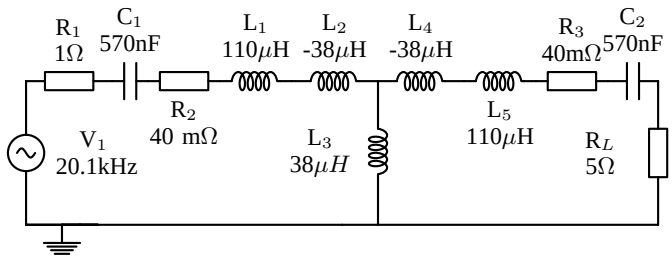

Fig. 14: Schematic of the equivalent network used for simulating WPT in the elementary cell

200, 330 and 400 the k is respectively 0.4955, 0.3581 and 0.2672. A viable frequency for this type of application is 20 kHz and the resulting capacitance for obtaining this resonant frequency is 575 nF.

We consider the complete MFIPT system in its stationary state and refer to the description in Section II. Fig. 14 shows the network implementing two mutually couple coils. We have assumed a Q=100 in order to maintain efficiency greater than 90% at resonance. In Fig. 15 we have plotted the efficiency of the two port network between the two 1 Ohm resistances.

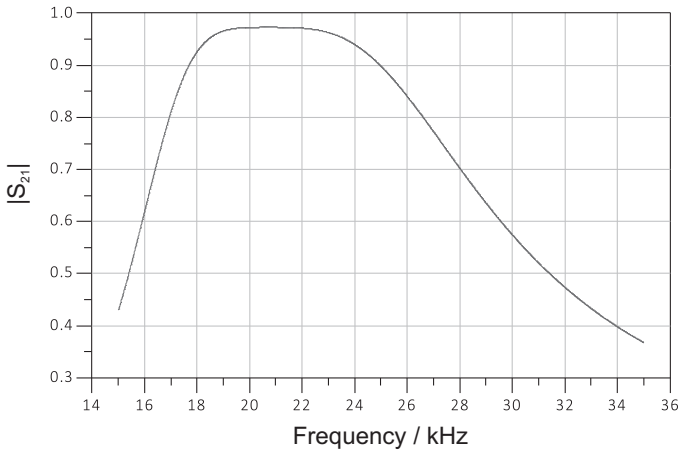

Fig. 15: Efficiency of the wireless power transfer network with an assumed Q of 100

In Fig. 16 the time dependence of the currents through the primary and secondary loops are displayed. It is noted that a switching frequency for the square wave generator of 20.1 kHz has been selected. Fig. 17 shows the voltages generated by the square wave source and the voltage amplitude at the load.

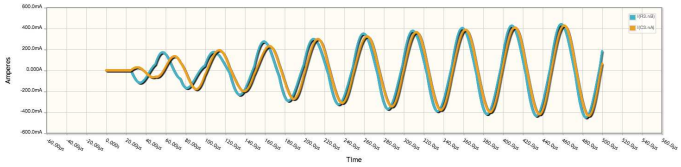

Fig. 16: Currents behavior at primary and secondary loops

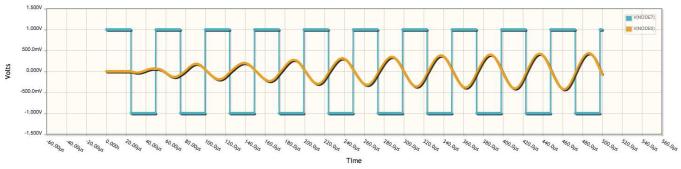

Fig. 17: Voltage across the load

VIII. Conclusion

The presented EV roadway powering system can be established by equipping a few highways with primary loop tracks. This allows unlimited roadway powering of EVs for long distance travels on the WLPT system equipped highways. Guidance of the vehicle along the primary coil track can be performed automatically. WLPT equipped EVs can coexist on the highways with conventional cars.

On minor roads, where vehicles usually are covering lower distances, they can drive battery powered. In regions where MFIPT tracks are not installed the vehicle batteries can be loaded via the IPT power stations on parking lots.

An electric vehicle embedded in a MFIPT system will exhibit an advanced cruise control system exchanging information also with other vehicles on the road and optimizing by this way energy consumption and traveling time. The equipment of highways with two or more primary coil tracks in one direction allowing to change the tracks and to pass other vehicles.

Acknowledgments

This is an extended version of the paper “A Bidirectional Moving Field Inductive Power Transfer System for Electric Vehicle” presented at the 11th International Conference on Telecommunications in Modern Satellite, Cable and Broadcasting Services – TELSIKS 2013, held in October 2013 in Niš, Serbia.

References

[1] R. Laouamer, M. Brunello, J. P. Ferrieux, O. Normand, and N. Buchheit, “A multi-resonant converter for non-contact charging with electromagnetic coupling,” in *Industrial Electronics, Control and Instrumentation, 1997. IECON 97. 23rd International Conference on*, vol. 2, 1997, pp. 792–797 vol.2.

[2] C.-S. Wang, G. Covic, and O. Stielau, "General stability criterions for zero phase angle controlled loosely coupled inductive power transfer systems," in *The 27th Annual Conference of the IEEE Industrial Electronics Society, 2001. IECON '01*, vol. 2, 2001, pp. 1049 –1054 vol.2.

[3] C.-S. Wang, O. Stielau, and G. Covic, "Design considerations for a contactless electric vehicle battery charger," *IEEE Transactions on Industrial Electronics*, vol. 52, no. 5, pp. 1308 – 1314, Oct. 2005.

[4] O. H. Stielau and G. A. Covic, "Design of loosely coupled inductive power transfer systems," in *Power System Technology, 2000. Proceedings. PowerCon 2000. International Conference on*, vol. 1, 2000, pp. 85–90 vol.1.

[5] C.-J. Chen, T.-H. Chu, C.-L. Lin, and Z.-C. Jou, "A study of loosely coupled coils for wireless power transfer," *Circuits and Systems II: Express Briefs, IEEE Transactions on*, vol. 57, no. 7, pp. 536–540, 2010.

[6] J. G. Bolger, F. Kirsten, and L. S. Ng, "Inductive power coupling for an electric highway system," in *28th IEEE Vehicular Technology Conference, 1978*, vol. 28, 1978, pp. 137–144.

[7] J. Bolger, L. S. Ng, D. Turner, and R. I. Wallace, "Testing a prototype inductive power coupling for an electric highway system," in *29th IEEE Vehicular Technology Conference, 1979*, vol. 29, 1979, pp. 48–56.

[8] H. Ayano, K. Yamamoto, N. Hino, and I. Yamato, "Highly efficient contactless electrical energy transmission system," in *IECON 02 [Industrial Electronics Society, IEEE 2002 28th Annual Conference of the]*, vol. 2, 2002, pp. 1364–1369 vol.2.

[9] M. L. G. Kissin, J. T. Boys, and G. A. Covic, "Interphase mutual inductance in polyphase inductive power transfer systems," *Industrial Electronics, IEEE Transactions on*, vol. 56, no. 7, pp. 2393–2400, 2009.

[10] A. Karalis, J. D. Joannopoulos, and M. Soljacic, "Efficient wireless non-radiative mid-range energy transfer," *Annals of Physics*, vol. 323, pp. 34–48, Apr. 2008.

[11] T. Imura, H. Okabe, and Y. Hori, "Basic experimental study on helical antennas of wireless power transfer for electric vehicles by using magnetic resonant couplings," in *Vehicle Power and Propulsion Conference, 2009. VPPC '09. IEEE*, 2009, pp. 936–940.

[12] Y. Hori, "Future vehicle society based on electric motor, capacitor and wireless power supply," in *Power Electronics Conference (IPEC), 2010 International*, 2010, pp. 2930–2934.

[13] M. Dionigi, A. Costanzo, and M. Mongiardo, "Network Methods for Analysis and Design of Resonant Wireless Power Transfer Systems," *Chapter of the book "Wireless Power Transfer-Principles and Engineering Explorations", http://www. intechweb. org*, 2011.

[14] J. A. Russer and P. Russer, "Design considerations for a moving field inductive power transfer system," in *IEEE International Wireles Power Transfer Conference Perugia WPTC*, May 15 - 16 2013, pp. 1–4.

[15] J. A. Russer, M. Dionigi, M. Mongiardo, and P. Russer, "A moving field inductive power transfer system for electric vehicles," in *Proc. 43rd European Microwave Conference EuMC*, Oct 2013, pp. 1–4.

[16] S. Nagai, H. Nagura, M. Nakaoka, and A. Okuno, "High-frequency inverter with phase-shifted PWM and load-adaptive PFM control strategy for industrial induction-heating," in *, Conference Record of the 1993 IEEE Industry Applications Society Annual Meeting, 1993*, 1993, pp. 2165–2172 vol.3.

[17] V. Garcia, M. Rico, J. Sebastian, M. Hernando, and J. Uceda, "An optimized DC-to-DC converter topology for high-voltage pulse-load applications," in *, 25th Annual IEEE Power Electronics Specialists Conference, PESC '94 Record*, 1994, pp. 1413–1421 vol.2.

[18] S. Nagai, E. Hiraki, Y. Arai, and M. Nakaoka, "New phase-shifted soft-switching PWM series resonant inverter topologies and their practical evaluations," in *, 1997 International Conference on Power Electronics and Drive Systems, 1997. Proceedings*, vol. 1, 1997, pp. 318–322 vol.1.

[19] J. Oliver, O. Garcia, P. Alou, and J. Cobos, "Analysis of the internal stability of two different control implementations of the phase-shifted full-bridge resonant converter," in *IEEE Power Electronics Specialists Conference, 2007. PESC*, 2007, pp. 737–741.

[20] A. Moradewicz and M. Kazmierkowski, "Contactless energy transfer system with FPGA-Controlled resonant converter," *IEEE Transactions on Industrial Electronics*, vol. 57, no. 9, pp. 3181–3190, 2010.

[21] J. Russer, M. Dionigi, M. Mongiardo, and P. Russer, "A bidirectional moving field inductive power transfer system for electric vehicles," in *11th International Confernce on Telecommunications in Modern Satellite, Cable and Broadcasting Services - TELSIKS*, Nis, Serbia, Oct 2013.

[22] T. Bieler, M. Perrottet, V. Nguyen, and Y. Perriard, "Contactless power and information transmission," in *Industry Applications Conference, 2001. Thirty-Sixth IAS Annual Meeting. Conference Record of the 2001 IEEE*, vol. 1, 2001, pp. 83–88 vol.1.

[23] Z. N. Low, R. Chinga, R. Tseng, and J. Lin, "Design and test of a high-power high-efficiency loosely coupled planar wireless power transfer system," *IEEE Transactions on Industrial Electronics*, vol. 56, no. 5, pp. 1801 –1812, May 2009.

[24] J.-J. Jang, W.-Y. Chae, H.-S. Kim, D.-G. Lee, and H.-J. Kim, "A study on optimization of the wireless power transfer using the half-bridge flyback converter," in *Computer Research and Development, 2010 Second International Conference on*, 2010, pp. 717–719.

[25] G. Doetsch, *Anleitung zum praktischen Gebrauch der Laplace–Transformation und der Z–Transformation*, 6th ed. Munich and Vienna: Oldenbourg, 1989.

[26] H. Bai and C. Mi, "Eliminate reactive power and increase system efficiency of isolated bidirectional dual-active-bridge DC–DC converters using novel dual-phase-shift control," *IEEE Transactions on Power Electronics*, vol. 23, no. 6, pp. 2905–2914, 2008.

[27] H. Xu, F. Peng, L. Chen, and X. Wen, "Analysis and design of Bi–directional Z–source inverter for electrical vehicles," in *Twenty-Third Annual IEEE Applied Power Electronics Conference and Exposition, 2008. APEC*, 2008, pp. 1252–1257.

[28] G. Ma, W. Qu, G. Yu, Y. Liu, N. Liang, and W. Li, "A zero-voltage-switching bidirectional DC–DC converter with state analysis and soft-switching-oriented design consideration," *IEEE Transactions on Industrial Electronics*, vol. 56, no. 6, pp. 2174–2184, 2009.

[29] F. Mastri, A. Costanzo, M. Dionigi, and M. Mongiardo, "Harmonic balance design of wireless resonant-type power transfer links," *Microwave Workshop Series on Innovative Wireless Power Transmission: Technologies, Systems, and Applications (IMWS), 2012 IEEE MTT-S International Microwave Symposium*, 2012.